ACS Sustainable Chemistry & Engineering

pubs.acs.org/journal/ascecg

Research Article

Ionic-liquid-Assisted Fabrication of Lignocellulosic Thin Films with Tunable Hydrophobicity

Kalavathy Rajan,* Keonhee Kim, Thomas J. Elder, Amit K. Naskar, and Nicole Labbé*

Cite This: https://doi.org/10.1021/acssuschemeng.2c01741

Read Online

ACCESS | Metrics & More | Article Recommendations | Supporting Information

ABSTRACT: Thin films with enhanced water repellency and mechanical strength can be fabricated from renewable lignocellulosic feedstock as a replacement for petrochemical-derived synthetic polymers, such that it minimizes life cycle impact on the environment and human health. In this study, hybrid poplar wood, either untreated (control) or pretreated with hot water at 160 °C for 20 min (HWE-20), 60 min (HWE-60), and 90 min (HWE-90), was dissolved in 1-ethyl-3-methylimidazolium acetate and regenerated to fabricate thin films. The HWE-90 films were enriched in lignin by 74%, specifically on the surface, which along with hemicellulose depletion imparted hydrophobicity (108° water contact angle) when compared to the control (56°), HWE-20 (77°), and HWE-60 (84°) films. They also exhibited 86% reduced water vapor sorption hysteresis and 75% improved storage modulus compared to the control. Thus, we demonstrate how to tune the lignocellulosic film properties via a combination of hot water pretreatment and ionic liquid dissolution.

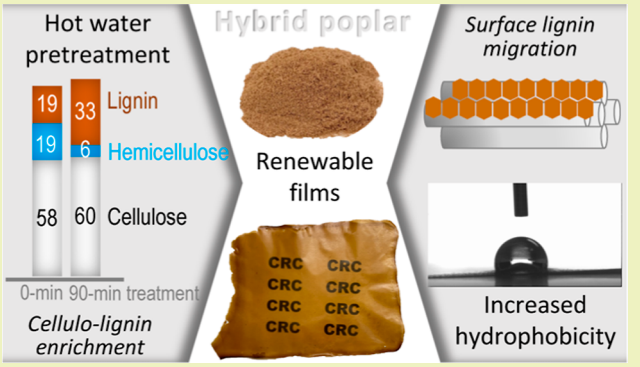

KEYWORDS: *hybrid poplar, hot water extraction, [EMIM][OAc], thin films, water contact angle*

INTRODUCTION

The global annual production of plastics was about 368 million tons in 2019,[1] and in the U.S. alone, the petrochemical industry annually consumes about 4.1 billion gallons of feedstock like naphtha, alkanes, olefins, and hydrocarbon gas liquids for the production of plastics and other synthetic polymers.[2] Consumption of these fossil fuel-derived feedstock leads to an emission of 81−287 million tons of CO_2 equivalent per year, which is one of the main sources of greenhouse gas emissions in the U.S. at 23%.[3] In addition to the production of greenhouse gases and the resulting contribution to climate change, utilization of synthetic polymers and plastics has other adverse impacts on the environment. The products of synthetic polymer degradation, namely, micro- and nano-plastics, are estimated to accumulate in the agricultural ecosystems at a rate of 0.3−6.3 kg m^{-2} in a human lifetime.[4] If the production and consumption of synthetic polymers continues at the current rate, there could be higher quantities of plastics than fish in the ocean by 2050, which will cause an irreversible damage to the ecosystem services.[5] Hence, development of biobased alternatives to petrochemical feedstock, which are net carbon neutral, biodegradable, and/or effectively recyclable, is of utmost importance.

Synthetic thin films and coatings used in sensors, smart devices, multiphase packaging, and biomedical applications are hard to replace because of their robust water resistance, thermo-stability, and specific structural order that proffers novel functionalities. However, recent studies have shown that natural polymers like cellulose, lignin, alginate, and chitosan could be successfully tuned to produce distinctive surface morphology and wetting behavior that have applications in barrier packaging,[6] drug delivery, wound healing,[7,8] and biosensors,[9] among others. Specifically, the inherent covalent linkages in lignin and structural polysaccharides could be exploited to achieve enhanced functionality and homogeneity. Lignocellulosic feedstock have been previously reported to improve interfacial compatibility and binding strength and tensile as well as barrier properties in composites, epoxy coatings, and biobased films.[10,11] Hence, if technologies are developed to directly utilize these feedstock, they will not only save on capital costs with processing and maintaining phase dispersions but also yield sustainable bioproducts with inherent environmental stability and resistance to mechanical deformation.

Lignocellulosic bioenergy feedstock, such as perennial grasses (switchgrass), short rotation woody crops (hybrid poplar), and agricultural residues (corn stover), have the

Received: March 23, 2022
Revised: June 13, 2022

potential to supply ~450 million tons of dry biomass annually in the U.S. for sustainable bioproduct manufacturing.[12−14] Our previous research has shown that whole lignocellulosic biomass, that is, hybrid poplar, could be successfully dissolved in ionic liquids like 1-ethyl-3-methylimidazolium acetate ([EMIM][OAc]) and regenerated to form thin films exhibiting a continuous 3D network with uniformly dispersed domains.[15] Initially, ionic liquids like [EMIM][OAc], 1-allyl-3-methylimidazolium chloride ([AMIM][Cl]), 1-butyl-3-methylimidazolium chloride, and [EMIM][Cl] were investigated to dissolve and cast cellulosic films by virtue of disrupting and substituting the natural intra- and inter-molecular hydrogen bonds between the elementary fibrils.[16−18] Later, dialkylimidazolium ionic liquids were demonstrated to achieve a near-complete dissolution of whole biomass, such as southern yellow pine, bagasse,[19] miscanthus,[20] beech,[21] poplar, and eucalyptus,[22] by virtue of hydrogen bond disruption, $\pi-\pi$ stacking with lignin aromatic rings, and formation of electron donor/electron acceptor complexes between cation, anion, and lignocellulose.[23,24] The direct dissolution of lignocellulosic biomass would facilitate downstream fractionation of cellulose and lignin for value addition[25] or manufacturing of biobased materials like films,[26,27] fibers,[24,28] and hydrogels.[29] Moreover, it is possible to potentially recover and reuse these ionic liquids.[30] Hence, they are an efficient tool to directly fabricate renewable thin films from whole lignocellulosic biomass.

Previous studies utilizing ionic liquids for biomaterial fabrication have expounded on the composition of solvent systems and dissolution temperature to (1) effectively regenerate cellulose or biomass dopes and (2) tune the resultant film's mechanical properties.[15−17] Also, in previous reports, biomass-based films were often fabricated from delignified substrates,[16,18] included additional solvents like DMSO, or artificially functionalized lignocellulose with vinyl groups to enable solution casting.[26,27] In the present study, we are demonstrating how to directly cast thin films from lignocellulosic biomass via a sequential autohydrolysis and ionic liquid-based dissolution process. And how the alteration of biomass chemical composition, and structural rearrangement of cellulose and lignin, could induce natural hydrophobicity in lignocellulosic films. To this end, we used [EMIM][OAc] and hybrid poplar wood as our model system and performed hot water pretreatment at different severities to induce biomass chemical compositional changes. Our results show how, despite the presence of hydroxyl groups, lignocellulosic biomass could yield hydrophobic thin films through ionic liquid-assisted induction of hierarchical networked structures. On a broader note, our investigation aims to elucidate the factors affecting advanced material fabrication using renewable lignocellulosic feedstock.

MATERIALS AND METHODS

Reagents and Lignocellulosic Biomass. The ionic liquid, ≥95% pure 1-ethyl-3-methylimidazolium acetate ([EMIM][OAc]), was purchased from IoLiTec GmbH (Heilbronn, Germany). Reagent-grade methanol and ethanol were purchased from Alfa-Aesar (Ward Hill, MA).

Hybrid poplar stem wood (*Populus trichocarpa* × *Populus maximowiczii*) was obtained from the Center for Renewable Carbon at the University of Tennessee, Knoxville; air-dried; and ground using a Wiley mill (Thomas Scientific, model #3383-L10, Swedesboro, NJ) to a particle size of <0.425 mm (40-mesh screen). The water and ethanol soluble extractives were removed from the ground biomass by following the NREL/TP-510-42619 protocol (National Renewable Energy Laboratory, Golden, CO). The extractives-free solids were air-dried and subjected to hot water pretreatment for partial hydrolysis of carbohydrates.

Hot Water Extraction. Hot water extraction (HWE) of the extractives-free hybrid poplar wood powder was conducted using ASE 350, an Accelerated Solvent Extractor (Dionex, Sunnyvale, CA), at 160 °C for 20, 60, and 90 min. The resultant solid hydrolysates are hereby denoted as HWE-*x*, where "*x*" signifies the duration of hot water treatment in minutes. The solid hydrolysate recovery was determined gravimetrically, based on the oven dry weight (ODW) of the starting material. An untreated control was also studied.

Solution Casting of Thin Films. The casting dopes were prepared by dissolving 5.5 g of control and 6.5 g of hot water pretreated hybrid poplar wood powder in 94.5 and 93.5 g of [EMIM][OAc], respectively, at 100 °C. The as-received ionic liquid had an equilibrium moisture content (MC) of 8.94 ± 0.72%, determined using a Pyris 1 thermogravimetric analyzer (TGA, PerkinElmer, Shelton, CT). An initial pre-heating step was employed at 100 °C for 30 min; as a result, its MC was reduced to 3.11 ± 0.53% (based on TGA). The pretreated solids were slowly added in stages to the pre-heated [EMIM][OAc] to facilitate uniform mixing. The dissolution process was monitored using a bright-field optical microscope at 10× magnification; the samples were deemed to be completely dissolved when no wood tissue was visible. The typical duration of biomass dissolution was between 12 and 18 days, depending on the hot water treatment severity.

Once the biomass was completely dissolved, the resulting dope was cooled down and maintained at 80 °C to fabricate thin films using the solution-casting technique. The dope was evenly spread on a glass plate to a thickness of 25 μm (for all HWE samples) or 40 μm (control) using a pre-calibrated casting knife. The control film was too brittle and needed to be cast at higher thickness to remain intact during the drying stage. After casting, the thin films were precipitated and regenerated in an anti-solvent bath composed of 100% methanol, incubated in de-ionized water for 1 h, sandwiched between metal mesh screens, and equilibrated in a series of humidity-controlled chambers at 21 °C to facilitate drying without sacrificing structural integrity. Relative humidities of 100, 95, 85, 75, and 54% were maintained in these chambers by using water and saturated solutions of KNO_3, KCl, NaCl, and $Mg(NO_3)_2$, respectively. The films were stabilized at 54% relative humidity for at least 24 h prior to any physical or mechanical analyses. The thin film yield was determined gravimetrically, in triplicate, after drying a representative sample in the oven at 105 °C for 16 h, as follows

$$\text{film yield} = \frac{m_{\text{film}}}{m_{\text{casting solution}} \times \text{percent}_{\text{dissolved biomass}}} \times 100 \quad (1)$$

The sustainability of our film fabrication process was estimated using the feedstock intensity factor,[31] defined as follows

$$\text{feedstock intensity factor} = \frac{m_{\text{raw material}}}{m_{\text{film}} + m_{\text{co-product}}} \quad (2)$$

where the liquid hot water hydrolysates are considered as co-products;[32] the lower the value of this factor, the higher will be the sustainability of operations.

Characterization of Wood Powder, Casting Solution, and Thin Films. *Chemical Compositional Analysis.* The structural carbohydrates, ash, acetyl, and lignin content of hybrid poplar wood powder and thin films were determined following the NREL/TP-510-42618 and TP-510-42622 protocols.[33,34] The films were shredded to a size of ≤4 mm^2 prior to the two-step hydrolysis using 72 and 4% (w/w) sulfuric acid. High-pressure liquid chromatography (HPLC) was employed to quantify the glucose, xylose, arabinose, galactose, and mannose content of the liquid hydrolyzate. The HPLC system was equipped with an Aminex HPX-87P analytical column (Bio-Rad Laboratories, Inc., Hercules, CA) and a refractive index detector (PerkinElmer, Shelton, CT). The acetyl content was measured using the same HPLC system but fitted with an Aminex HPX-87H analytical column, where glacial acetic acid purchased from Alfa Aesar

https://doi.org/10.1021/acssuschemeng.2c01741
ACS Sustainable Chem. Eng. XXXX, XXX, XXX−XXX

Table 1. Chemical Composition of Untreated and Hot Water Pretreated Hybrid Poplar Wood[a]

		chemical composition[c] (% ODW)					
sample ID	HWE severity[b]	cellulose	hemicellulose[d]	lignin[e]	acetyl	ash	post-HWE biomass recovery[c] (% ODW)
control	n/a	44.1 ± 0.1	20.5 ± 0.2	28.5 ± 0.3	6.2 ± 0.2	0.6 ± 0.1	n/a
HWE-20	5.8	47.5 ± 0.3	17.9 ± 0.3	29.4 ± 0.8	5.1 ± 0.3	0.5 ± 0.1	90.1 ± 1.1
HWE-60	6.3	54.4 ± 0.2	13.1 ± 0.2	29.9 ± 0.7	3.6 ± 0.4	0.2 ± 0.1	79.1 ± 1.5
HWE-90	6.5	57.7 ± 0.3	10.9 ± 0.2	29.8 ± 0.4	2.2 ± 0.1	0.3 ± 0.1	74.6 ± 0.9

[a]Hot water extraction (HWE) was conducted at 160 °C for 0, 20, 60, or 90 min; ODW—oven dry weight. [b]Combined severity factor = log R_0 + | pH-7|, where R_0 = time × $e^{(\text{temp}_{\text{reaction}}-100)/14.75}$ (Chum et al., 1990). [c]Means and standard deviations are determined for N = 3. [d]Hemicellulose is the sum of xylan, arabinan, galactan, and mannan. [e]Lignin is the sum of acid soluble and acid insoluble (Klason) lignin.

(Haverhill, MA) was used as the calibration standard. The solid residues were adjusted for inorganic content and used to calculate the acid insoluble lignin content. The absorbance of liquid hydrolyzate at 240 nm was used to calculate the acid soluble lignin content.[33]

Rheological Properties. The casting solution's dynamic viscosity was measured in triplicate using an AR-G2 stress-controlled rheometer (TA Instruments, New Castle, DE), fitted with a cone and plate geometry of 40 mm diameter, 2° cone angle, and 56 μm truncation. Samples, protected by perimeter application of silicon oil and metal plate covers, were subjected to steady state shear at a rate of 0.1−100 s^{-1} and at 80 °C.

Physico-chemical Properties. The density of the thin films was determined by accurately weighing excised squares of 1 cm × 1 cm and known thickness (0.022 mm for HWE films and 0.040 mm for the control) measured using a screw gauge.

Changes in inherent linkages of hybrid poplar biomass and resulting films were determined using 2D-HSQC (heteronuclear single quantum coherence) nuclear magnetic resonance (NMR) spectroscopy. About 50 mg of the thin films was first soaked in 650 μL of a DMSO-d_6/pyridine-d_5 (4:1 v/v) solvent mixture for 5 h, pulverized into a gel-like consistency, and then carefully transferred into thin-walled quartz tubes of 5 mm diameter for analysis.[35] For wood powder, about 50 mg was transformed into a homogenous gel by using the above-stated NMR solvent mixture and sonicating in a water bath for 5 h. Quantitative and qualitative HSQC measurements of the resulting gels were obtained in 8 scans (with a longer recycle delay) and 32 scans per increment (~1.5 h), respectively, using a 600 MHz NMR instrument fitted with a cryoprobe. The 2D $^1H/^{13}C$ HSQC acquisition parameters published by Mansfield et al. were followed,[35] and data processing was conducted using Mnova v14.2 software (Mestrelab Research S.L., Santiago, Spain). The DMSO-d_6 cross-peak signal at (δC/δH) 39.5/2.5 ppm was used as a reference, and the sample spectra were processed by applying a baseline correction (third-order Bernstein polynomial fit), manual phase corrections, Gaussian and exponential apodization (F1: 90 Hz/−10 Hz, F2: 10 Hz/−0.5 Hz), and a spectrum size of 1024 (along t1 and t2). For quantification, all cross-peaks were integrated and normalized to the pyridine-d_5 peak at (δC/δH) 123.8/7.2 ppm.

Fourier transform infrared (FTIR) spectra of the thin films (equilibrated at 54% relative humidity) were collected using a Spectrum Two spectrometer (PerkinElmer, Shelton, CT) fitted with a universal attenuated total reflectance (diamond crystal) accessory; the scanning specifications were 4 cm^{-1} resolution, 16 scans per spectrum, and 5 spectra per film. The collected spectra were detrended using second-order polynomial function and normalized using standard normal variate method, prior to principal component analysis (PCA) using the Unscrambler X v10.4 software (Aspen Technology, Inc., Bedford, MA). PCA, a multivariate analytical method, was applied to the FTIR spectra to detect any significant differences, similarities, or trends in chemical signatures. Grouping in the PCA scores will indicate samples with similar chemical features, whereas the PCA loadings will identify major spectral bands responsible for such grouping.

Morphological Properties. Atomic force microscopy (AFM) was conducted in a tapping mode using an Asylum Research Cypher S system (Oxford Instruments America Inc., Concord, MA) fitted with a AC200TS silicon probe. A standard cantilever in air with a resonance frequency of ~286 kHz and stiffness of k = 40 N m^{-1} was used. The scan area per film was 5 μm^2, and the line scan rate was 1 Hz. The topography data were collected from two independent locations for each treatment, at ambient temperature, and processed using Igor Pro 9.0 software (WaveMetrics Inc., Lake Oswego, OR).

Thermo-mechanical Properties. Dynamic mechanical analysis (DMA) of the thin film samples with average dimensions of 6.5 × 4.25 mm was carried out using a DMA-Q800 instrument (TA instruments, New Castle, DE). Samples were pre-conditioned at 54% relative humidity and analyzed at a constant strain mode, where the temperature was ramped from 21 to 300 °C at a rate of 3 °C/min, 1 Hz frequency, and 5 μm displacement. The preload strain was set at 0.01 N.

The Pyris 1 TGA was used to measure the change in MC of neat [EMIM][OAc] by heating a 10 mg sample from 50 to 100 °C, under air, at a rate of 20 °C/min and by holding it at 100 °C for 30 min. To determine the thermal degradation properties of thin films, about 2 mg samples were heated from 25 to 700 °C, at a rate of 10 °C/min, under nitrogen. The DMA and TGA measurements were conducted in duplicate. Statistical analysis, namely, comparison of means using Tukey−Kramer HSD test and multivariate correlation, was conducted using the JMP 16 software (SAS Institute, Cary, NC).

Dynamic Vapor Sorption and Static Contact Angle Studies. Water vapor sorption and desorption was determined gravimetrically, where the dry films were first incubated in a series of increasing relative humidities, that is, 54, 75, 85, 95, and 100% and then in the reverse order, at 21 °C. The film weight was recorded manually, at predetermined intervals for several weeks, until the sorption−desorption isotherms were built. The MC, on an ODW basis, was determined based on the equilibrated weight of films in each relative humidity chamber. Hysteresis was then calculated based on the difference in MC for a specific relative humidity,[36] as given below

$$\text{absolute hysteresis (\%)} = \text{MC}_{\text{desorption}} - \text{MC}_{\text{sorption}} \quad (3)$$

Hydrophobicity of the thin films was determined using a model 100-00 contact angle goniometer (Rame-Hart instrument Co., Succasunna, NJ). About 2 μL of sessile water droplets, generated at a rate of 10 μL/min, were placed on even surfaces and the contact angle was measured after equilibration. All analyses were conducted at 21 °C, where the surface tension of water was about 72.3 mN m^{-1}. The average of six measurements was reported for both the water contact angle (WCA) and water vapor sorption experiments.

RESULTS AND DISCUSSION

Effect of HWE on Biomass Physico-chemical Properties and Ionic Liquid Dissolution. The chemical composition of untreated and HWE hybrid poplar biomass is presented in Table 1. The HWE conditions were selected based on previous reports, where the pretreatment of poplar species at 160 °C, between 15 and 90 min, facilitated the maximization of xylan recovery without significantly hydrolyzing lignin and cellulose.[37,38] As given in Table 1, increase in HWE severity led to a corresponding decrease in the recovery of pretreated solids, from 10 to 25%. Other studies have also

https://doi.org/10.1021/acssuschemeng.2c01741
ACS Sustainable Chem. Eng. XXXX, XXX, XXX−XXX

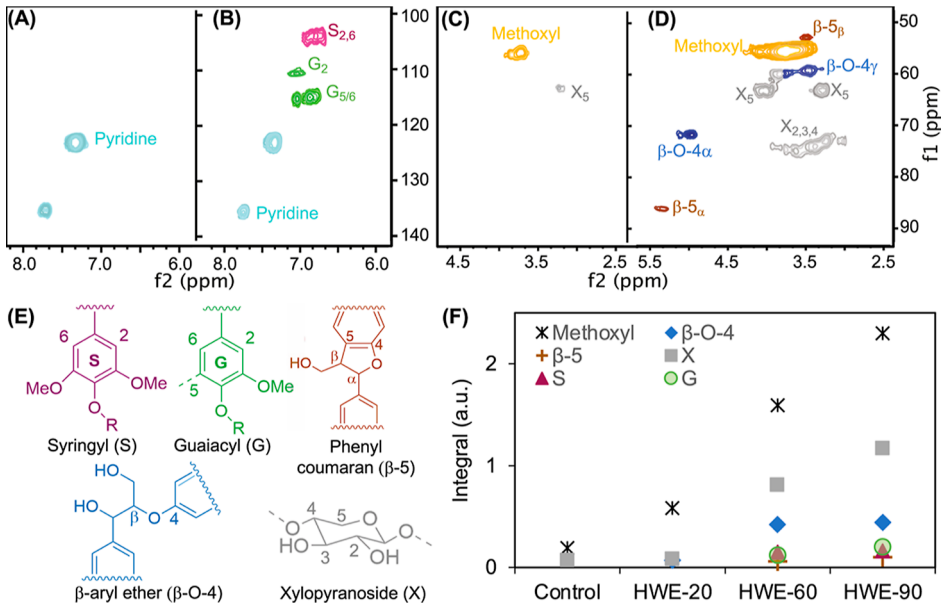

Figure 1. Aromatic regions of (A) control and (B) HWE-90 hybrid poplar biomass determined using quantitative 2D-HSQC NMR; side-chain regions of (C) control and (D) HWE-90 biomass; (E) legend for substructures identified in the 2D-HSQC NMR spectra; (F) normalized cross-peak integrals of substructures in control and HWE biomass at 160 °C for 20 min (HWE-20), 60 min (HWE-60), and 90 min (HWE-90). The corresponding chemical shift assignments are provided in the Supporting Information, Table S1.

reported a mass loss of 25−48% during hot water pretreatment of hardwoods.[39] Hot water pretreatment enables the reduction in recalcitrance of lignocellulosic feedstock via (i) deacetylation of matrix polymers by hydronium ions and subsequent autohydrolysis by the released acetic acid;[40] (ii) reduction in molecular weight of residual hemicellulose and the degree of polymerization of cellulose;[41] and (iii) cleavage of native ether linkages in lignin.[41] In the present study, HWE resulted in the solubilization and removal of hemicellulosic polysaccharides by up to 61% and lignin loss by up to 23%. Since both lignin and hemicellulose form a matrix surrounding the cellulose fiber bundles and contribute toward the recalcitrance of plant biomass,[42] partial autohydrolysis of these fractions would enhance biomass accessibility for ionic liquid dissolution.

HWE has been previously reported to improve the dissolution of wood chips in ionic liquids like tetrabutylphosphonium acetate[43] and [EMIM][OAc][39] via (i) cleaving lignin−hemicellulose linkages[42] and (ii) exposing the hydroxyl groups of cellulose, hemicellulose, and lignin to ionic liquids. The acetate anion of the ionic liquids then forms a strong hydrogen bond with the exposed hydroxyl groups and facilitates the dissolution of pretreated biomass.[43] The pressurized conditions of HWE also enhances the penetration of ionic liquid into lignocellulosic biomass via increasing the porosity and fibrillation.[39] Therefore, we applied HWE to facilitate the complete dissolution of hybrid poplar wood in [EMIM][OAc].

Our study results showed that the application of HWE improved the amount of hybrid poplar biomass soluble in [EMIM][OAc] by 20% (i.e., from 5.8 to 6.95% w/w) compared to the untreated control. The effects of HWE on hybrid poplar's chemical structure could be elucidated using 2D-HSQC NMR spectroscopy. The cross-peak signals of control and HWE-90 biomass observed by quantitative 2D NMR analyses are provided in Figure 1A−D, and the spectra of HWE-20 and HWE-60 biomass are provided in the Supporting Information, Figure S1. The cross-peaks were integrated and normalized to the pyridine signal and are presented in Figure 1F. It is evident from Figure 1F that the total amount of measurable inter-unit (β-O-4, β-5) and aromatic linkages (syringyl, guaiacyl) in lignin, as well as the number of polysaccharide (xylopyranoside) substructures, increased significantly from control to HWE-90 biomass as a function of increasing HWE severity. As a result of hot water pretreatment, under identical NMR acquisition parameters, several chemical structures of the biomass were rendered accessible/measurable. As shown in Figure 1F, only the methoxyl and xylopyranoside groups are measurable in the control, while additional lignin β-O-4 linkages are measurable in HWE-20. Linkages like β-5 and aromatic units in lignin are measurable in HWE-60, whereas the HWE-90 biomass exhibited 16-fold higher polysaccharide structures, 11-fold more methoxyl groups, and 100% more aromatic, β-O-4, and β-5 inter-unit linkages when compared to the control. The increase in quantifiable/accessible xylopyranoside units in HWE-60 and HWE-90 biomass aligns well with the previous report that hot water pretreatment could increase the access of ionic liquids to the hydroxyl groups of polysaccharides and thus enhance biomass dissolution.[43] Our study additionally shows that the changes rendered to lignocellulosic biomass even at low HWE severity, such as the increase in access to lignin methoxyl groups in HWE-20, are sufficient to improve biomass solubility in [EMIM][OAc]. Thus, based on the chemical compositional analysis (Table 1) and 2D-HSQC NMR results, we can conclude that both the partial solubilization of matrix polymers and increase in access to labile functional groups, as a result of HWE, enhance biomass dissolution in ionic liquid.

Effect of HWE on Film Yield and Physico-chemical Properties. The HWE process affected both the chemical composition and yield of hybrid poplar thin films, as shown in Figure 2. The yield of films, which is expressed as a mass fraction of the original biomass (eq 1), increased as a function of HWE severity, from 51% for control to 71% for HWE-90

https://doi.org/10.1021/acssuschemeng.2c01741
ACS Sustainable Chem. Eng. XXXX, XXX, XXX−XXX

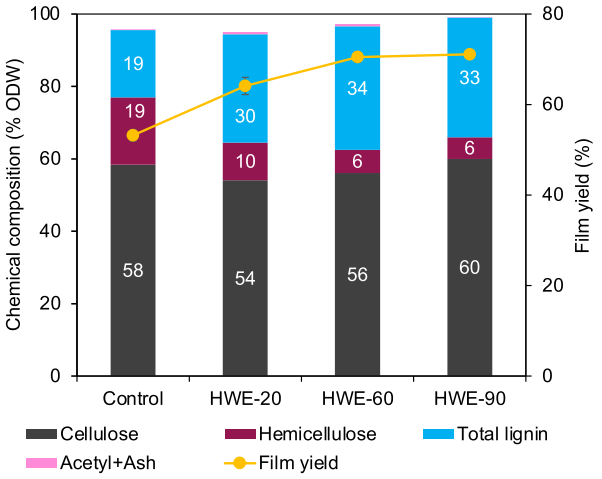

Figure 2. Chemical composition and yield of thin films regenerated from hybrid poplar wood after dissolution in [EMIM][OAc]. The biomass was extracted with hot water at 160 °C for 0 min (control), 20 min (HWE-20), 60 min (HWE-60), and 90 min (HWE-90). All measurements are provided on an ODW basis for $N = 3$.

treatment. The control film lost about 65% of lignin during dissolution and regeneration from [EMIM][OAc], whereas the HWE films experienced only 17−26% lignin loss. Previous studies have shown that pretreatment of poplar wood with [EMIM][OAc] led to a lignin loss of 30%, due to the formation of strong hydrogen bonds between acetate anion and lignin, thereby retaining it in a solution state and preventing its regeneration.[44] Moreover, lignin's interaction radii with methanol, the regeneration solvent, is relatively higher compared to cellulose or hemicellulose, and hence, some lignin may be solubilized during the film regeneration stage.[15] The higher retention of lignin in HWE films could be attributed to the presence of the relatively insoluble phenylcoumaran (β-5) and resinol ($\beta-\beta'$) substructures.[45] The 2D-HSQC NMR analysis of HWE-60 and -90 films demonstrated the presence of resinol ($\beta-\beta'$) substructures, in addition to oxidized syringyl units (Figure S2), that are characteristic to that of lignocellulosic biomass subjected to HWE and ionic liquid dissolution.[45,46] Apart from inducing lignin structural changes, the film fabrication process also selectively deacetylated and dissolved ≤68% of the hemicellulosic polysaccharides in the HWE films compared to the control (Figure 2). Thus, as a result of lignin retention and selective hemicellulose dissolution, our HWE films were enriched in lignin, while the cellulose content remained nearly the same.

Another important effect of HWE, and the subsequent changes in hybrid poplar biomass composition, is its impact on the casting solution's viscosity (Figure S4). A strong positive correlation (Pearson's $r = 0.93$) existed between the ratio of cellulose and lignin over hemicellulose (C + L/HC) in the biomass and the dope viscosity (Tables 2 and S2). Our previous research showed that increasing the concentration of dissolved hybrid poplar biomass (≥4% w/w) as well as a subsequent rise in dope viscosity was essential to induce molecular entanglements between cellulose and lignin.[24] The current study shows that the partial removal of hemicellulosic sugars also leads to an increase in the casting solution's viscosity, perhaps due to the enhanced mobility and accessibility of cellulose fiber bundles and lignin, causing polymer−polymer and polymer−ionic liquid interactions via hydrogen bonding.[23,24] In the end, as a result of changes in dope viscosity, the density of our films was also affected (Table 2). A higher dope viscosity was strongly correlated to an increase in film density (Pearson's $r = 0.93$), which once again delineates the significant impact of biomass composition on the process of film casting as well as the end product properties.

The HWE pretreatment also impacted the film morphology; as seen in Figure 3A−D, all hybrid poplar films were translucent, but the HWE-60 and HWE-90 films were notably darker in color owing to their enrichment in lignin. The surface roughness increased as a function of HWE severity (Figure 3E−H); the root-mean-square averages of the profile heights (R_q), over an evaluation length of 5 μm, for the control, HWE-20, HWE-60, and HWE-90 films were 10.5 ± 3.4, 26.2 ± 0.4, 38.2 ± 1.2, and 45.9 ± 2.7 nm, respectively. This increase in surface roughness could be directly correlated to the enrichment of cellulose and lignin (C + L/HC) in the films (Pearson's $r = 0.94$). Previous reports have also shown that films made from a physical mixture of nanocellulose and lignin exhibited a roughness factor of 27−50 nm.[47,48] The topography of our HWE films closely resembled wood powder membranes, regenerated from a tetrabutylammonium acetate and DMSO solvent system, where a heterogeneous mixture of cellulose fibrils of 100−400 nm dimension and globular lignin nanoparticles was observed.[49] Moreover, only the control film exhibited uniform peaks of 10−20 nm in diameter with occasional heterogeneous phases of ≤400 nm (Figure 3I). All HWE films exhibited peaks of 270−700 nm in diameter (Figures 3J−L), which could correspond to fibrillated cellulosic bundles. The severely pretreated biomass films (HWE-60 and -90) also exhibited globular features of ∼10 nm in diameter (Figure 3G,H), which could be lignin nanoparticles;[47,49] additional characterization using techniques like nano-FTIR is required for a more direct elucidation.

Effect of Film Composition on Thermo-mechanical Properties. X-ray diffraction studies showed that the cellulose crystalline domains of the hybrid poplar films were character-

Table 2. Physico-chemical Properties of Casting Solution and Regenerated Films from Hybrid Poplar Wood Dissolved in [EMIM][OAc]

sample name	(C + L)/HC in biomass[a]	dynamic viscosity of the dope at 80 °C[b,c] (mPa s)	density of thin films (kg/m^3)	crystallinity index (%)	ultimate tensile strength[d] (MPa)	elongation at break[d] (%)
control	3.5 ± 0.4	189.4 ± 4.2	265.2 ± 14.1	61.2 ± 0.8	22.1 ± 2.2	2.2 ± 0.0
HWE-20	4.3 ± 0.9	234.8 ± 3.5	280.5 ± 32.7	63.1 ± 1.4	33.7 ± 4.5	2.3 ± 0.6
HWE-60	6.4 ± 0.7	312.4 ± 0.7	308.7 ± 24.4	59.7 ± 0.8	40.0 ± 2.0	4.6 ± 0.2
HWE-90	8.1 ± 0.5	659.3 ± 2.4	334.8 ± 31.4	56.8 ± 1.3	32.2 ± 1.6	5.8 ± 1.0

[a]C—cellulose; L—total lignin; HC—hemicellulose content of hybrid poplar biomass. [b]Measured at 0.1 s^{-1} shear rate. [c]Biomass concentration in [EMIM][OAc] was 5.8% (w/w) for control and 6.95% (w/w) for HWE samples. [d]Mean and standard deviations are presented for $N = 6$.

https://doi.org/10.1021/acssuschemeng.2c01741
ACS Sustainable Chem. Eng. XXXX, XXX, XXX−XXX

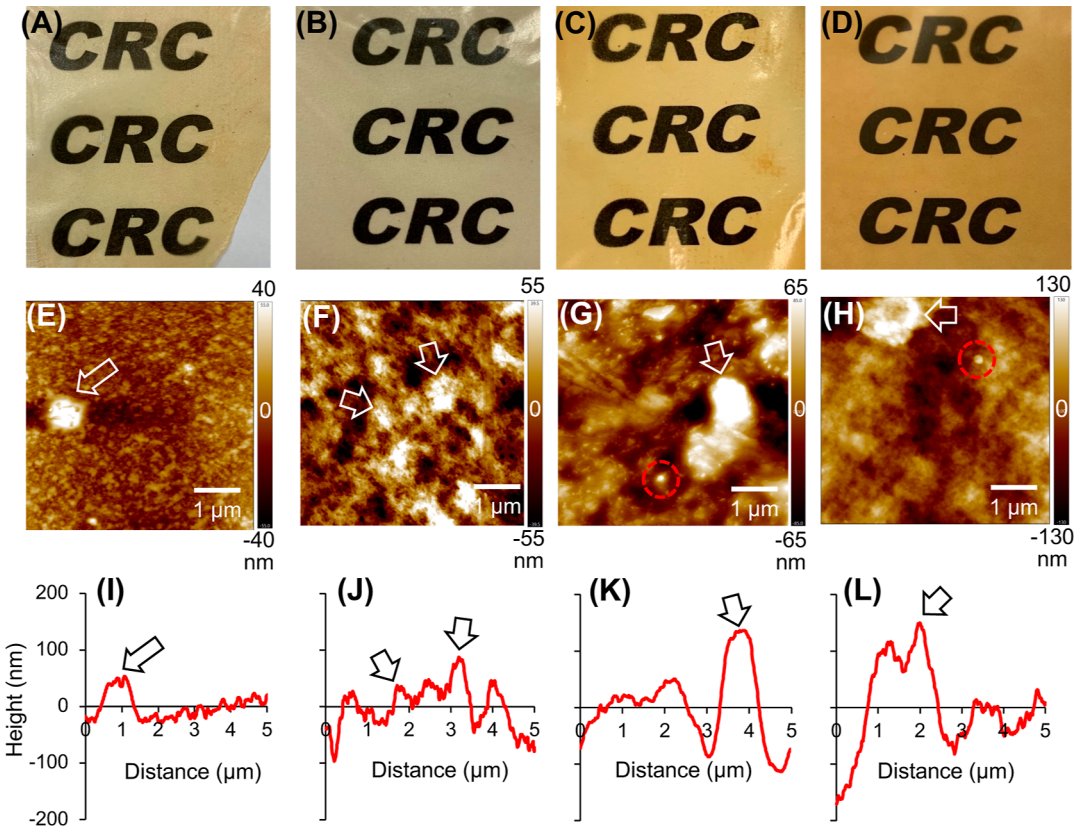

Figure 3. Bulk appearance of hybrid poplar films (7 × 6 cm^2) is depicted in the top row; AFM images with the corresponding height scale are provided in the middle row; cross-sectional roughness profiles, across 5 μm, are provided in the bottom row. Legend: images (A,E,I) correspond to the control film; (B,F,J) correspond to HWE-20 film; (C,G,K) correspond to HWE-60 film; and (D,H,L) correspond to HWE-90 film.

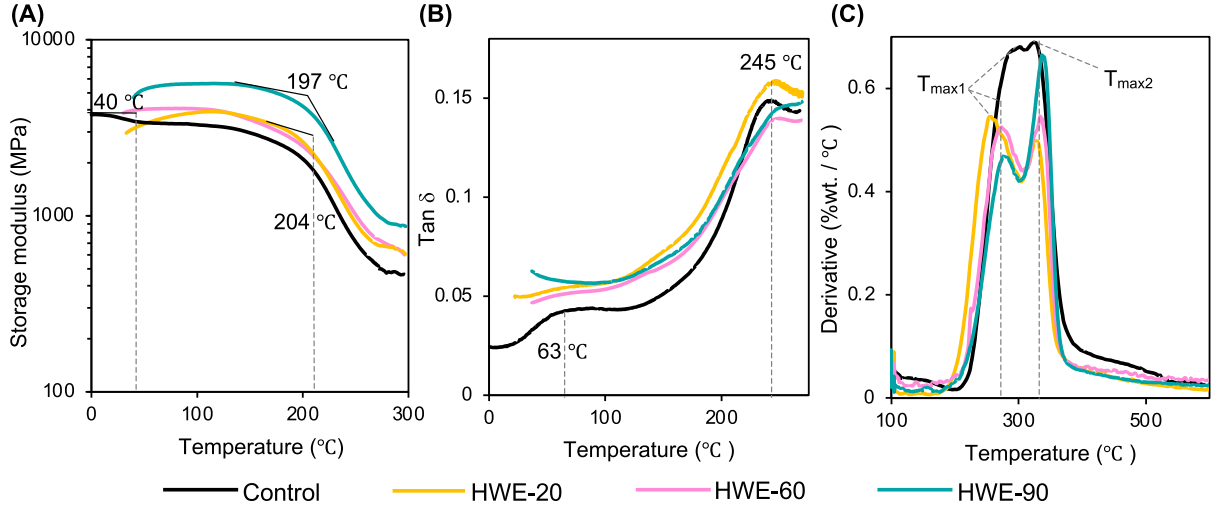

Figure 4. (A) Storage modulus and (B) loss tangent (tan δ curves) of hybrid poplar thin films determined via DMA at a constant frequency of 1 Hz; (C) derivative thermograms of films prepared from control and hot water-treated hybrid poplar at 160 °C for 20 min (HWE-20), 60 min (HWE-60), and 90 min (HWE-90).

istic to that of cellulose-II polymorph, exhibiting 2θ peaks at 12 and 20.6° corresponding to (1-10) and (110) planes, respectively (Figure S5). Considering the high crystallinity index (57−63%), our films were not as strong at ≤40 MPa (Table 2), which we attribute to the significant presence of amorphous lignin. Similar ultimate tensile strength of 30−38 MPa have been reported for regenerated bagasse films that contained a mixture of cellulose and lignin.[27] The amorphous lignin fraction, in addition to affecting film stiffness, could also introduce flexibility (even better than crystalline cellulose) and act as a plasticizer.[50] Hence, enrichment in lignin led to the improvement of elongation at break of HWE-60 and -90 films (Table 2 and Figure S6). Previous reports have also shown that the presence of plasticizers such as sorbitol and glycerol could enhance the tensile properties of regenerated cellulose films.[51]

The enrichment of cellulose and lignin had a significant impact on the viscoelastic behavior of pretreated samples, as shown in Figure 4A,B. The storage moduli (E') of HWE-60

https://doi.org/10.1021/acssuschemeng.2c01741
ACS Sustainable Chem. Eng. XXXX, XXX, XXX−XXX

Table 3. Dynamic Mechanical and Thermal Degradation Properties of Thin Films Cast from Hybrid Poplar Biomass Dissolved in [EMIM][OAc]

			thermal degradation properties			
sample name	T_α [a] (°C)	T_g [b] (°C)	mass loss at 105 °C (%)	T_{max1} [c] (°C)	T_{max2} [c] (°C)	Char residues (%) @700 °C
control	170.9 ± 10.2^{B}	240.8 ± 1.5^{A}	26.6 ± 0.1	295.2 ± 1.5	329.0 ± 1.8	8.2 ± 1.9
HWE-20	184.6 ± 0.3^{AB}	244.7 ± 0.9^{A}	12.0 ± 0.1	254.8 ± 0.6	330.1 ± 0.7	12.2 ± 2.1
HWE-60	194.2 ± 1.2^{AB}	248.7 ± 1.9^{A}	11.8 ± 0.0	273.7 ± 1.8	332.3 ± 2.6	16.2 ± 0.1
HWE-90	208.0 ± 7.2^{A}	256.2 ± 10.8^{A}	10.4 ± 0.5	280.6 ± 2.4	338.4 ± 1.4	18.5 ± 1.3

[a]Calculated from storage modulus (E'). [b]Calculated from the peak of loss tangents; the means were compared using Tukey–Kramer HSD test, and the values denoted by different alphabets were significantly different at $\alpha = 0.05$. [c]T_{max}—temperature corresponding to the maximum rate of weight loss in the films.

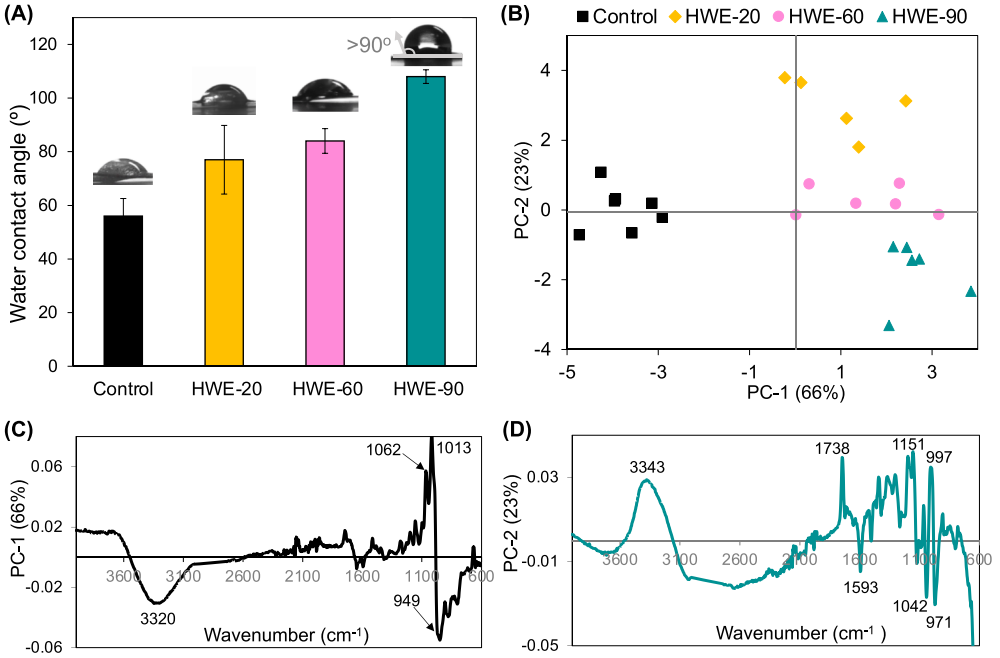

Figure 5. (A) WCA of hybrid poplar thin films; (B) PCA of the films' FTIR spectra and the corresponding scores plot; (C) loadings plot for PC-1; (D) loadings plot for PC-2.

(~4 GPa) and HWE-90 (~5.6 GPA) films were significantly higher than the control (~3 GPA) in the temperature range of 30–150 °C (Figure 4A), which is unsurprising because these films contained 17–21% more cellulose and lignin. The reported moduli (E') of our hybrid poplar films are superior to that of microcrystalline cellulose films (5.5 kPa), also regenerated from [EMIM][OAc], and comparable to cross-linked chitosan films (4–8 GPa).[52,53] As given in Table 3, the HWE films undergo an alpha transition (T_α) around 185–208 °C, followed by a rubbery plateau, which is characteristic to that of cross-linked or entangled polymeric materials. However, considering the very high T_g of the rigid lignin phase (>200 °C) and the temperature range (275–300 °C) at which these films reached a modulus plateau, it may be wise to assume that the lignin fraction might have undergone partial degradation in the rubbery region. Nonetheless, the steady plateau of storage modulus (Figure 4A) suggests a robustness of our films that maintained a networked structure. In the case of the control (Figure 4A), there was a beta transition onset at about 40 °C, which could correspond to the liberation of methanol trapped during the regeneration process. The evaporation of methanol was also captured by the broad peak at around 63 °C in the tan δ curve (Figure 4B). The peak of loss tangent could be used to calculate the glass transition temperature, T_g, which was not significantly different between the control, HWE-20, HWE-60, and HWE-90 films (Table 3). While the high T_g values are indicative of molecular weights larger than purified cellulose or lignin,[54] the broad and overlapping glass transition regions in all treatments is indicative of a polydisperse system.

The thermal degradation behavior was distinctly different between the control and HWE films, as shown in Figure 4C and indicated in Table 3. There were two distinct regions of maximum degradation rates (T_{max1} and T_{max2}) in HWE-20, -60, and -90 samples as opposed to the control, which had a broad, indistinguishable peak maxima. Previous research has shown that severe ionic liquid pretreatment could cause the splitting of thermal degradation rates because (1) depolymerization of major polymers like cellulose and lignin lowers T_{max1} and (2) further condensation of lignin and cellulose degradation products raises T_{max2}.[55] Overall, our hybrid poplar films exhibited higher thermal stability than [AMIM][Cl]-regenerated microcrystalline cellulose (260 °C) or cellulose acetate films (197 °C).[17,26]

Effect of Film Structure and Physico-chemical Properties on Water Repellency. Water repellent lignocellulosic films with tunable tensile strength and elongation as described in the previous sections could find applications in

https://doi.org/10.1021/acssuschemeng.2c01741
ACS Sustainable Chem. Eng. XXXX, XXX, XXX–XXX

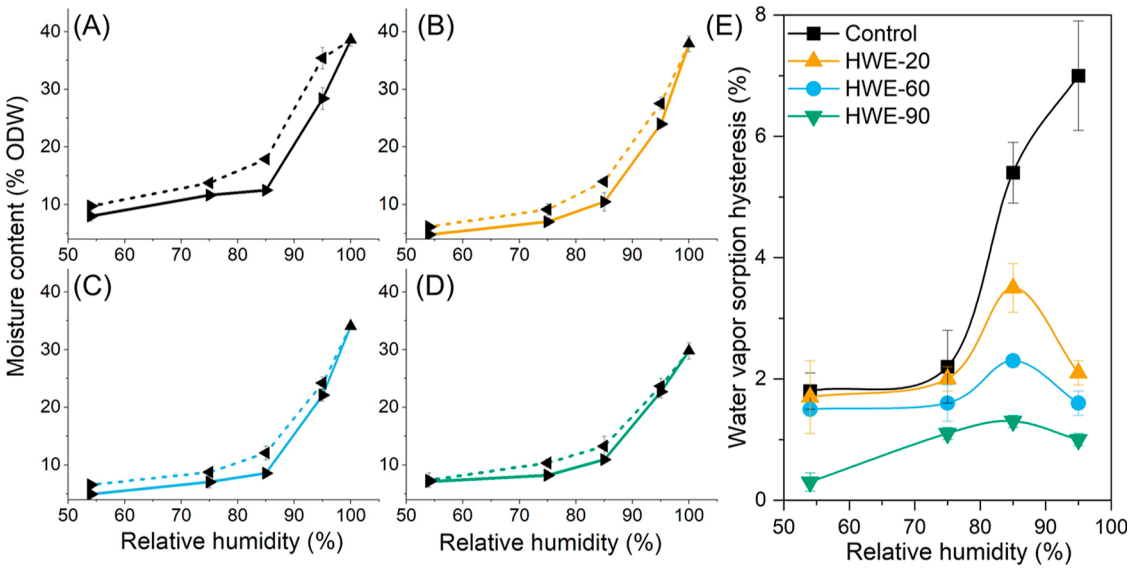

Figure 6. Sorption (solid lines) and desorption (dotted lines) isotherms of (A) control, (B) HWE-20, (C) HWE-60, and (D) HWE-90 films at 21 °C; (E) effect of relative humidity on absolute hysteresis between the sorption and desorption isotherms of thin films at 21 °C. Mean and standard deviations are provided for $N = 6$.

multilayered barrier packaging.[6] Hence, we tested the control and our HWE films for WCA as well as dynamic water vapor sorption. The control film exhibited a WCA of 56° (Figure 5A), meaning it is hydrophilic, similar to that of ionic liquid welded nanocellulosic films.[56] The HWE films, on the other hand, exhibited significantly higher WCA, ranging from 77 to 108° (Figure 5A). Specifically, HWE-90 exhibited a WCA of 108°, which means that these films have low wettability. The hydrophobicity of HWE-90 films is a noteworthy achievement, as it is higher than that of ionic liquid-based cotton linter films (WCA = 75°) and comparable to that of silane-coated wood surfaces (WCA ≥ 100°).[51,57] The high surface roughness of HWE-90 could have contributed to its hydrophobicity (Figure 3H,L).[48] Moreover, it was depleted in hemicellulose while simultaneously enriched in lignin content, which could have ultimately induced hydrophobicity.

The surface chemical property of the films was characterized by FTIR spectroscopy, and the resulting spectra were subjected to PCA, a multivariate method for classifying various treatment groups based on their chemical signatures. The PCA scores provided in Figure 5B show that the HWE film spectra are clearly separated from the control by principal component 1 (PC-1). As previously discussed, the HWE films were enriched in cellulose and lignin, and hence, their FT-IR spectra also exhibited C−O valence vibrations belonging to both cellulose (C_3-O_3H) and lignin ($C_{alkyl}-O$ ether), as evidenced in the PC-1 loadings (Figure 5C).[58] On the other hand, the control film exhibited more O−H valence vibrations as well as pyran ring vibrations corresponding to 3320 and 949 cm^{-1}, respectively, which could be the reason why these films are more hygroscopic. Among the pretreated films, HWE-90 exhibited higher number of lignin signatures at 1593 and 1042 cm^{-1} corresponding to aromatic skeletal vibration and $C_{alkyl}-O$ ether vibrations, respectively, than cellulose signature of C−O valence vibration at 971 cm^{-1} [principal component 2 (PC-2) loadings in Figure 5D]. In the case of HWE-20 and HWE-60 films, more O−H valence vibrations (3343 cm^{-1}), unconjugated C═O stretch (1738 cm^{-1}), and C−O valence vibrations (997 cm^{-1}) were detected, characteristic to that of cellulose (Figure 5D). These results show how the HWE-90 film transpired to exhibit a hydrophobic surface, with respect to WCA, by virtue of higher lignin and fewer OH groups on the surface.

The water vapor sorption and desorption isotherms of all films (Figure 6A−D) exhibited a hysteresis characteristic to that of mesoporous structures with slit-shaped pores (IUPAC Type H3).[59] The equilibrium moisture gain at 100% relative humidity was ≤40% (Figure 6A−D), which is similar to that of regenerated nanocellulose films with a cellulose-II structure.[60] The absolute hysteresis between the sorption and desorption isotherms, at a specific relative humidity, was calculated according to eq 3 and is provided in Figure 6E. Sorption hysteresis is commonly attributed to the swelling and irreversible relaxation of a polymer network, resulting from the rupture of intermolecular hydrogen bonding.[61] Our HWE-90 films exhibited the least amount of hysteresis compared to other treatments, which could be attributed to its significantly lower water wettability, which not only limits water vapor sorption but could also facilitate desorption. The hysteresis in the control films displayed an increasing trend that reached a sharp peak at about 95% relative humidity (Figure 6E), which is similar to that of cellulose fibers that are susceptible to swelling upon exposure to high moisture conditions.[60] On the other hand, the HWE-20 and -60 films exhibited moderate hysteresis that peaked at 85% relative humidity, which is similar to that of regenerated films enriched in crystalline cellulose II.[60] The overall sorption hysteresis behavior of our hybrid poplar films was superior to [EMIM][OAc]-treated cellulose paper (9−11%);[62] the performance of HWE films was specifically comparable to that of phenol resin-treated pinewood veneers (1−5%).[63]

Sustainability of Lignocellulosic Films. Because these films are entirely made of lignocellulosic biomass, they are 100% renewable and could be recycled using the ionic liquid. Our proposed process encompasses sustainable technologies such as hot water pretreatment, which does not require any chemical input and produces a hemicellulose-rich co-product with direct utility as a prebiotic ingredient, among others.[32]

https://doi.org/10.1021/acssuschemeng.2c01741
ACS Sustainable Chem. Eng. XXXX, XXX, XXX−XXX

The anti-solvents (methanol, water) used during solution casting are non-hazardous and could be recovered via distillation and reused. The ionic liquid could also be recovered via rotovaporation,[19] or pervaporation,[64] and recycled for up to four biomass treatment cycles before losing its efficacy.[30] Based on these assumptions and eq 2, the sustainability of HWE-90 film, our best water repellent product, was compared to that of plastics and other biobased films used in packaging and mulching applications. As shown in Table 4, the HWE-90 films are more sustainable in terms of

Table 4. Comparing the Sustainability of Hybrid Poplar Films with Commercial Products

sustainability metric	polylactide film[a]	polypropylene film[a]	linear low density polyethylene film[a]	HWE-90 film[b]
feedstock intensity factor	1.45	1.66	1.12	1.04

[a]Values are referenced from Lokesh et al. (2020).[31] [b]For every 1 g of HWE-90 film, the amount of raw material used and value added co-products generated were 1.41 and 0.35 g, respectively.

achieving a near-complete utilization of hybrid poplar biomass. The process feasibility could be further improved by reusing the ionic liquid and by increasing the amount of dissolved lignocellulosic biomass.

Overall, the films prepared in this study show tunable physico-chemical characteristics including material composition, thermal stability, mechanical property, and water vapor sorption and desorption capability, as a function of hot water pretreatment severity. This suggests a tremendous potential for designing renewable films and fibers from whole lignocellulosic biomass by deploying an ionic liquid-based partial deconstruction and plasticization process. The hydrophobicity of the lignin-rich HWE-90 films, along with high elastic modulus and dimensional stability ($T_g \sim 256$ °C), can help to develop sustainable water repellent materials. Natural fiber-based reinforcements find limited applications due to discontinuity in filament length, high porosity, and moisture sorption that creates problem with composite fabrication. Results from this research can help to mitigate these issues if continuous fibers or films, which are water and moisture repellent, could be manufactured from whole or waste lignocellulosic biomass.

CONCLUSIONS

This study elucidates how HWE enhances hybrid poplar dissolution in [EMIM][OAc], improves the resulting film yield, and enriches their cellulose and lignin composition at the cost of hemicellulose content. HWE also has a latent impact on film density and surface orientation of OH groups, which ultimately induces water repellence. Moreover, utilization of whole lignocellulosic biomass provided several advantages: water repellence on par with expensive silylated products, tensile strength and storage modulus on par with cross-linked polymers, and higher thermo-tolerance than cellulose-only films. In future, we will explore the process sustainability via designing continuous fabrication methods and determining techno-economic feasibility.

ASSOCIATED CONTENT

Supporting Information

The Supporting Information is available free of charge at https://pubs.acs.org/doi/10.1021/acssuschemeng.2c01741.

Images of 2D-HSQC and ^{1}H NMR, XRD, rheometry, and stress−strain relationship of hybrid poplar biomass and thin films; methodology for ultimate tensile test and XRD of lignocellulosic films; and data tables for δC/δH NMR assignments and statistical correlation matrix of physico-chemical properties of hybrid poplar biomass and thin films (PDF)

AUTHOR INFORMATION

Corresponding Authors

Kalavathy Rajan − *Center for Renewable Carbon, The University of Tennessee, Knoxville, Tennessee 37996, United States;* orcid.org/0000-0002-1837-1235; Phone: +1(865)946-1129; Email: krajan@utk.edu

Nicole Labbé − *Center for Renewable Carbon, The University of Tennessee, Knoxville, Tennessee 37996, United States;* orcid.org/0000-0002-2117-4259; Phone: +1(865)946-1126; Email: nlabbe@utk.edu

Authors

Keonhee Kim − *Center for Renewable Carbon, The University of Tennessee, Knoxville, Tennessee 37996, United States*

Thomas J. Elder − *USDA-Forest Service, Southern Research Station, Auburn, Alabama 36849, United States;* orcid.org/0000-0003-3909-2152

Amit K. Naskar − *Carbon and Composites Group, Chemical Sciences Division, Oak Ridge National Laboratory, Oak Ridge, Tennessee 37831, United States;* orcid.org/0000-0002-1094-0325

Complete contact information is available at: https://pubs.acs.org/10.1021/acssuschemeng.2c01741

Author Contributions

The manuscript was written through contributions of all authors. All authors have given approval to the final version of the manuscript.

Funding

The research efforts were supported in part by the US Forest Service Award (19-JV-594 1130131-026) and by the USDA-NIFA's Agriculture and Food Research Initiative Award (2018-67009-27375) and HATCH grant (TEN00510).

Notes

The authors declare no competing financial interest.

ACKNOWLEDGMENTS

The authors acknowledge Dr. Roger B. Proksch, at the University of Tennessee—Advanced Microscopy and Imaging Center, Knoxville, TN, for conducting the AFM analysis of lignocellulosic films. The authors also acknowledge Dr. Donald Stec at Vanderbilt's Small Molecule NMR Facility, Nashville, TN, for conducting the 2D-HSQC NMR analyses and Drs. Teng Li and Tao Wu of the Department of Food Science, University of Tennessee, Knoxville, TN, for providing instrumentation access for contact angle analysis.

REFERENCES

(1) Meunier, B. Plastics—the Facts 2020. https://www.statista.com/statistics/282732/global-production-of-plastics-since-1950/ (accessed Sept 21).

(2) EIA. U.S. Refinery Net Production of Petrochemical Feedstocks (Thousand Barrels). https://www.eia.gov/dnav/pet/hist/LeafHandler.ashx?n=PET&s=MPCRX_NUS_1&f=M (accessed Sept 14).

(3) EPA. U.S. Greenhouse Gas Emissions from the Industrial Sector, by Category, 2019. https://cfpub.epa.gov/ghgdata/inventoryexplorer/index.html#industry/entiresector/allgas/category/current (accessed Sept, 21 2019).

(4) Ng, E.-L.; Huerta Lwanga, E.; Eldridge, S. M.; Johnston, P.; Hu, H.-W.; Geissen, V.; Chen, D. An overview of microplastic and nanoplastic pollution in agroecosystems. *Sci. Total Environ.* **2018**, *627*, 1377−1388.

(5) Banks, I.; De Smet, M.; Murphy, J.; Steventon, P.; Rodger, S. *The New Plastics Economy: Rethinking the Future of Plastics*; Ellen MacArthur Foundation: Geneva, Switzerland, 2016; pp 1−36.

(6) Chemin, M.; Heux, L.; Guérin, D.; Crowther-Alwyn, L.; Jean, B. Hybrid gibbsite nanoplatelet/cellulose nanocrystal multilayered coatings for oxygen barrier improvement. *Front. Chem.* **2019**, *7*, 507.

(7) Maver, T.; Mohan, T.; Gradišnik, L.; Finšgar, M.; Stana Kleinschek, K.; Maver, U. Polysaccharide thin solid films for analgesic drug delivery and growth of human skin cells. *Front. Chem.* **2019**, *7*, 217.

(8) Zou, T.; Sipponen, M. H.; Österberg, M. Natural shape-retaining microcapsules with shells made of chitosan-coated colloidal lignin particles. *Front. Chem.* **2019**, *7*, 370.

(9) Gestranius, M.; Otsuka, I.; Halila, S.; Hermida-Merino, D.; Solano, E.; Borsali, R.; Tammelin, T. High-resolution patterned biobased thin films via self-assembled carbohydrate block copolymers and nanocellulose. *Adv. Mater. Interfaces* **2020**, *7*, 1901737.

(10) Nair, S. S.; Kuo, P.-Y.; Chen, H.; Yan, N. Investigating the effect of lignin on the mechanical, thermal, and barrier properties of cellulose nanofibril reinforced epoxy composite. *Ind. Crops Prod.* **2017**, *100*, 208−217.

(11) Rojo, E.; Peresin, M. S.; Sampson, W. W.; Hoeger, I. C.; Vartiainen, J.; Laine, J.; Rojas, O. J. Comprehensive elucidation of the effect of residual lignin on the physical, barrier, mechanical and surface properties of nanocellulose films. *Green Chem.* **2015**, *17*, 1853−1866.

(12) Langholtz, M. H.; Stokes, B. J.; Eaton, L. M. *Billion-ton Report: Advancing Domestic Resources for a Thriving Bioeconomy; ORNL/TM-2016/160*; Oak Ridge National Laboratory: Oak Ridge, TN, 2016; p 448.

(13) Paul, S.; Dutta, A.; Thimmanagari, M.; Defersha, F. Techno-economic assessment of corn stover for hybrid bioenergy production: A sustainable approach. *Therm. Eng.* **2019**, *13*, 100408.

(14) Sands, R. D.; Malcolm, S. A.; Suttles, S. A.; Marshall, E. *Dedicated Energy Crops and Competition for Agricultural Land, ERR-223*; U.S. Department of Agriculture, Economic Research Service: Washington, D.C., 2017; pp 1−72.

(15) Wang, J.; Boy, R.; Nguyen, N. A.; Keum, J. K.; Cullen, D. A.; Chen, J.; Soliman, M.; Littrell, K. C.; Harper, D.; Tetard, L.; Rials, T. G.; Naskar, A. K.; Labbé, N. Controlled assembly of lignocellulosic biomass components and properties of reformed materials. *ACS Sustainable Chem. Eng.* **2017**, *5*, 8044−8052.

(16) Nor Amalini, A.; Noor Haida, M. K.; Imran, K.; Mohamad Haafiz, M. K. Relationship between dissolution temperature and properties of oil palm biomass based-regenerated cellulose films prepared via ionic liquid. *Mater. Chem. Phys.* **2019**, *221*, 382−389.

(17) Pang, J.; Liu, X.; Zhang, X.; Wu, Y.; Sun, R.; Sun, R.-C. Fabrication and characterization of regenerated cellulose films using different ionic liquids. *J. Spectrosc.* **2014**, *6*, 1270.

(18) Turner, M. B.; Spear, S. K.; Holbrey, J. D.; Rogers, R. D. Production of bioactive cellulose films reconstituted from ionic liquids. *Biomacromolecules* **2004**, *5*, 1379−1384.

(19) Li, W.; Sun, N.; Stoner, B.; Jiang, X.; Lu, X.; Rogers, R. D. Rapid dissolution of lignocellulosic biomass in ionic liquids using temperatures above the glass transition of lignin. *Green Chem.* **2011**, *13*, 2038−2047.

(20) Padmanabhan, S.; Kim, M.; Blanch, H. W.; Prausnitz, J. M. Solubility and rate of dissolution for Miscanthus in hydrophilic ionic liquids. *Fluid Phase Equilib.* **2011**, *309*, 89−96.

(21) Zavrel, M.; Bross, D.; Funke, M.; Büchs, J.; Spiess, A. C. High-throughput screening for ionic liquids dissolving (ligno-)cellulose. *Bioresour. Technol.* **2009**, *100*, 2580−2587.

(22) Fort, D. A.; Remsing, R. C.; Swatloski, R. P.; Moyna, P.; Moyna, G.; Rogers, R. D. Can ionic liquids dissolve wood? Processing and analysis of lignocellulosic materials with 1-n-butyl-3-methylimidazolium chloride. *Green Chem.* **2007**, *9*, 63−69.

(23) Rajan, K.; Elder, T.; Abdoulmoumine, N.; Carrier, D. J.; Labbé, N. Understanding the in situ state of lignocellulosic biomass during ionic liquids-based engineering of renewable materials and chemicals. *Green Chem.* **2020**, *22*, 6748−6766.

(24) Nguyen, N. A.; Kim, K.; Bowland, C. C.; Keum, J. K.; Kearney, L. T.; André, N.; Labbé, N.; Naskar, A. K. A fundamental understanding of whole biomass dissolution in ionic liquid for regeneration of fiber by solution-spinning. *Green Chem.* **2019**, *21*, 4354−4367.

(25) Sun, N.; Rahman, M.; Qin, Y.; Maxim, M. L.; Rodríguez, H.; Rogers, R. D. Complete dissolution and partial delignification of wood in the ionic liquid 1-ethyl-3-methylimidazolium acetate. *Green Chem.* **2009**, *11*, 646−655.

(26) Nishita, R.; Kuroda, K.; Suzuki, S.; Ninomiya, K.; Takahashi, K. Flame-retardant plant thermoplastics directly prepared by single ionic liquid substitution. *Polym. J.* **2019**, *51*, 781−789.

(27) Chen, M.; Zhang, X.; Liu, C.; Sun, R.; Lu, F. Approach to renewable lignocellulosic biomass film directly from bagasse. *ACS Sustainable Chem. Eng.* **2014**, *2*, 1164−1168.

(28) Sun, N.; Li, W.; Stoner, B.; Jiang, X.; Lu, X.; Rogers, R. D. Composite fibers spun directly from solutions of raw lignocellulosic biomass dissolved in ionic liquids. *Green Chem.* **2011**, *13*, 1158−1161.

(29) Berton, P.; Shen, X.; Rogers, R. D.; Shamshina, J. L. High-molecular-weight chitin and cellulose hydrogels from biomass in ionic liquids without chemical crosslinking. *Ind. Eng. Chem. Res.* **2019**, *58*, 19862−19876.

(30) Weerachanchai, P.; Lee, J.-M. Recyclability of an ionic liquid for biomass pretreatment. *Bioresour. Technol.* **2014**, *169*, 336−343.

(31) Lokesh, K.; Matharu, A. S.; Kookos, I. K.; Ladakis, D.; Koutinas, A.; Morone, P.; Clark, J. Hybridised sustainability metrics for use in life cycle assessment of bio-based products: resource efficiency and circularity. *Green Chem.* **2020**, *22*, 803−813.

(32) Rajan, K.; D'Souza, D. H.; Kim, K.; Choi, J. M.; Elder, T.; Carrier, D. J.; Labbé, N. Production and characterization of high value prebiotics from biorefinery-relevant feedstocks. *Front. Microbiol.* **2021**, *12*, 675314.

(33) Sluiter, A.; Hames, B.; Ruiz, C.; Scarlata, C.; Sluiter, J.; Templeton, D.; Crocker, D. *Determination of Structural Carbohydrates and Lignin in Biomass*; National Renewable Energy Laboratory: Golden (CO), 2012; pp 1−18.

(34) Sluiter, A.; Hames, B.; Ruiz, R.; Scarlata, C.; Sluiter, J.; Templeton, D. *Determination of Ash in Biomass*; National Renewable Energy Laboratory: Golden (CO), 2005; pp 1−8.

(35) Mansfield, S. D.; Kim, H.; Lu, F.; Ralph, J. Whole plant cell wall characterization using solution-state 2D NMR. *Nat. Protoc.* **2012**, *7*, 1579−1589.

(36) Cordin, M.; Griesser, U. J.; Bechtold, T. Analysis of moisture sorption in lyocell-polypropylene composites. *Cellulose* **2017**, *24*, 1837−1847.

(37) Martin, E. M.; Bunnell, K. A.; Lau, C.-S.; Pelkki, M. H.; Patterson, D. W.; Clausen, E. C.; Smith, J. A.; Carrier, D. J. Hot water and dilute acid pretreatment of high and low specific gravity Populus deltoides clones. *J. Ind. Microbiol. Biotechnol.* **2011**, *38*, 355−361.

https://doi.org/10.1021/acssuschemeng.2c01741
ACS Sustainable Chem. Eng. XXXX, XXX, XXX−XXX

(38) Seibert-Ludwig, D.; Hahn, T.; Hirth, T.; Zibek, S. Selection and optimization of a suitable pretreatment method for Miscanthus and poplar raw material. *GCB Bioenergy* **2019**, *11*, 171−180.
(39) Hauru, L. K. J.; Ma, Y.; Hummel, M.; Alekhina, M.; King, A. W. T.; Kilpeläinen, I.; Penttilä, P. A.; Serimaa, R.; Sixta, H. Enhancement of ionic liquid-aided fractionation of birchwood. Part 1: Autohydrolysis pretreatment. *RSC Adv.* **2013**, *3*, 16365−16373.
(40) Garrote, G.; Domínguez, H.; Parajó, J. C. Study on the deacetylation of hemicelluloses during the hydrothermal processing of Eucalyptus wood. *Eur. J. Wood Wood Prod.* **2001**, *59*, 53−59.
(41) Li, M.; Cao, S.; Meng, X.; Studer, M.; Wyman, C. E.; Ragauskas, A. J.; Pu, Y. The effect of liquid hot water pretreatment on the chemical-structural alteration and the reduced recalcitrance in poplar. *Biotechnol. Biofuels* **2017**, *10*, 237.
(42) Blumentritt, M.; Gardner, D. J.; Cole, B. J. W.; Shaler, S. M. Influence of hot-water extraction on ultrastructure and distribution of glucomannans and xylans in poplar xylem as detected by gold immunolabeling. *Holzforschung* **2016**, *70*, 243−252.
(43) Deb, S.; Labafzadeh, S. R.; Liimatainen, U.; Parviainen, A.; Hauru, L. K. J.; Azhar, S.; Lawoko, M.; Kulomaa, T.; Kakko, T.; Fiskari, J.; Borrega, M.; Sixta, H.; Kilpeläinen, I.; King, A. W. T. Application of mild autohydrolysis to facilitate the dissolution of wood chips in direct-dissolution solvents. *Green Chem.* **2016**, *18*, 3286−3294.
(44) Gschwend, F. J. V.; Hallett, J. P.; Brandt-Talbot, A. Exploring the effect of water content and anion on the pretreatment of poplar with three 1-ethyl-3-methylimidazolium ionic liquids. *Molecules* **2020**, *25*, 2318.
(45) Zhang, L.; Yan, L.; Wang, Z.; Laskar, D. D.; Swita, M. S.; Cort, J. R.; Yang, B. Characterization of lignin derived from water-only and dilute acid flowthrough pretreatment of poplar wood at elevated temperatures. *Biotechnol. Biofuels* **2015**, *8*, 203.
(46) Brandt, A.; Chen, L.; van Dongen, B. E.; Welton, T.; Hallett, J. P. Structural changes in lignins isolated using an acidic ionic liquid water mixture. *Green Chem.* **2015**, *17*, 5019−5034.
(47) Gerbin, E.; Rivière, G. N.; Foulon, L.; Frapart, Y. M.; Cottyn, B.; Pernes, M.; Marcuello, C.; Godon, B.; Gainvors-Claisse, A.; Crônier, D.; Majira, A.; Österberg, M.; Kurek, B.; Baumberger, S.; Aguié-Béghin, V. Tuning the functional properties of lignocellulosic films by controlling the molecular and supramolecular structure of lignin. *Int. J. Biol. Macromol.* **2021**, *181*, 136−149.
(48) Bian, H.; Gao, Y.; Wang, R.; Liu, Z.; Wu, W.; Dai, H. Contribution of lignin to the surface structure and physical performance of cellulose nanofibrils film. *Cellulose* **2018**, *25*, 1309−1318.
(49) Miao, J.; Yu, Y.; Jiang, Z.; Tang, L.; Zhang, L. Partial delignification of wood and membrane preparation using a quaternary ammonium ionic liquid. *Sci. Rep.* **2017**, *7*, 42472.
(50) Nagardeolekar, A.; Ovadias, M.; Dongre, P.; Bujanovic, B. Prospects and challenges of using lignin for thermoplastic materials. In *Lignin Utilization Strategies: From Processing to Applications*; Yoo, C. G., Ragauskas, A., Eds.; American Chemical Society: Washington, D.C., 2021; pp 231−271. DOI: 10.1021/bk-2021-1377.ch010
(51) Pang, J.; Liu, X.; Zhang, X.; Wu, Y.; Sun, R. Fabrication of cellulose film with enhanced mechanical properties in ionic liquid 1-allyl-3-methylimidazolium chloride (AmimCl). *Materials* **2013**, *6*, 1270−1284.
(52) Khouri, J.; Penlidis, A.; Moresoli, C. Viscoelastic properties of crosslinked chitosan films. *Process* **2019**, *7*, 157.
(53) Zhang, M.; Ding, C.; Chen, L.; Huang, L. The preparation of cellulose/collagen composite films using 1-ethyl-3-methylimidazolium acetate as a solvent. *BioResources* **2014**, *9*, 756−771.
(54) Tao, J.; Hosseinaei, O.; Delbeck, L.; Kim, P.; Harper, D. P.; Bozell, J. J.; Rials, T. G.; Labbé, N. Effects of organosolv fractionation time on thermal and chemical properties of lignins. *RSC Adv.* **2016**, *6*, 79228−79235.
(55) Zhang, J.; Feng, L.; Wang, D.; Zhang, R.; Liu, G.; Cheng, G. Thermogravimetric analysis of lignocellulosic biomass with ionic liquid pretreatment. *Bioresour. Technol.* **2014**, *153*, 379−382.
(56) Niu, X.; Huan, S.; Li, H.; Pan, H.; Rojas, O. J. Transparent films by ionic liquid welding of cellulose nanofibers and polylactide: Enhanced biodegradability in marine environments. *J. Hazard. Mater.* **2021**, *402*, 124073.
(57) Tang, Z.; Xie, L.; Hess, D. W.; Breedveld, V. Fabrication of amphiphobic softwood and hardwood by treatment with non-fluorinated chemicals. *Wood Sci. Technol.* **2017**, *51*, 97−113.
(58) Schwanninger, M.; Rodrigues, J. C.; Pereira, H.; Hinterstoisser, B. Effects of short-time vibratory ball milling on the shape of FT-IR spectra of wood and cellulose. *Vib. Spectrosc.* **2004**, *36*, 23−40.
(59) Sing, K. S. W.; Everett, D. H.; Haul, R. A. W.; Moscou, L.; Pierotti, R. A.; Rouquerol, J.; Siemieniewska, T. Reporting physiosorption data for gas/solid systems with special reference to the determination of surface area and porosity. *Pure Appl. Chem.* **1985**, *57*, 603−619.
(60) Guo, X.; Wu, Y.; Xie, X. Water vapor sorption properties of cellulose nanocrystals and nanofibers using dynamic vapor sorption apparatus. *Sci. Rep.* **2017**, *7*, 14207.
(61) Fredriksson, M.; Thybring, E. E. Scanning or desorption isotherms? Characterising sorption hysteresis of wood. *Cellulose* **2018**, *25*, 4477−4485.
(62) Korpela, A.; Tanaka, A.; Khakalo, A.; Orelma, H. Water sorption properties of regenerated sulfate pulp paper treated with ionic liquid [EMIM]OAc. *J. Wood Chem. Technol.* **2020**, *40*, 306−316.
(63) Hosseinpourpia, R.; Adamopoulos, S.; Mai, C. Dynamic vapour sorption of wood and holocellulose modified with thermosetting resins. *Wood Sci. Technol.* **2016**, *50*, 165−178.
(64) Sun, J.; Shi, J.; Murthy Konda, N. V. S. N.; Campos, D.; Liu, D.; Nemser, S.; Shamshina, J.; Dutta, T.; Berton, P.; Gurau, G.; Rogers, R. D.; Simmons, B. A.; Singh, S. Efficient dehydration and recovery of ionic liquid after lignocellulosic processing using pervaporation. *Biotechnol. Biofuels* **2017**, *10*, 154.

https://doi.org/10.1021/acssuschemeng.2c01741
ACS Sustainable Chem. Eng. XXXX, XXX, XXX−XXX